Sizing Optimization and Energy Management Strategy for Hybrid Energy Storage System Using Multiobjective Optimization and Random Forests

Mince Li, *Student Member, IEEE*, Li Wang, *Student Member, IEEE*, Yujie Wang, *Member, IEEE*, and Zonghai Chen, *Senior Member, IEEE*

***Abstract*—Sizing optimization and energy management strategy (EMS) are two key points for the application of the hybrid energy storage system (HESS) in electric vehicles. This article aims to conduct the sizing optimization of HESS and apply an adaptive real-time EMS for practice. First, considering the system cost and battery lifespan, the multiobjective grey wolf optimizer is used to obtain the Pareto front. Second, with optimal parameters, the offline optimal power splitting results by dynamic programming (DP) under different driving patterns are analyzed. Then, the random forests (RF) method is used to learn control rules from the DP results. Driving pattern recognition (DPR) is implemented by the support vector machine (SVM). The intelligent EMS is composed of RF to guide power distribution and SVM to realize DPR. Finally, a combined load cycle involving different driving patterns is used for verification. Results illustrate that the proposed adaptive RF-based EMS can demonstrate a notable superiority in terms of battery protection, ultra-capacitor utilization, and system efficiency. Compared with the ordinary RF-based EMS without DPR, the proposed method can reduce total energy loss by 0.74%–9.49%, and reduce the battery Ah-throughput by 0.5%–19.83% under unknown driving cycles.**

***Index Terms*—Energy management strategy (EMS), hybrid energy storage system (HESS), multiobjective grey wolf optimizer (GWO), random forests (RF), sizing optimization.**

I. Introduction

ELECTRIC vehicles (EVs) are playing an urgent part in solving the problems of energy shortage and environmental pollution [1]. Lithium batteries have become the mainstream energy storage system of EVs due to their outstanding energy density. However, the large current spike and surge power shocks in real applications would exacerbate battery degradation [2].

As a most promising solution, ultracapacitors (UCs) have been proposed to construct the hybrid energy storage system (HESS) with batteries [3]. UCs have advantages such as long cycle life, low internal resistance, and high power density, which are complementary to batteries [4]. The HESS composed of the UC and the battery has become a research hotspot. Researchers have proposed several topologies of HESS, which can be divided into three categories: fully active topology, semiactive topology, and passive topology [5]. Due to superior performance and relatively low cost, the semiactive topology is the best tradeoff between complexity control and capital cost [6]. The UC system is connected with a dc/dc converter in UC semiactive HESS topology, and battery is connected to dc bus directly. The dc bus voltage is stable but the requirements for dc/dc converters are even more stringent due to the wide voltage range of the UC system. The battery system is decoupled in battery semiactive HESS topology, bringing the benefit of easier control for battery. However, the voltage on the dc bus will vary continuously within a certain range [2], [5]. Each of the two topologies has its own advantages and disadvantages, and in this work, the battery semiactive topology is chosen to make the battery more convenient to control. When the system topology has been determined, there are two crucial points for the practical application of HESS. The first one is the components sizing optimization to meet the real-world driving conditions and extend the life of the battery at the lowest possible cost. The other issue is the application of energy management strategy (EMS) to reduce energy waste and make full use of the ability of batteries and UCs.

The current component sizing of HESS in the literature can be classified into two categories: analysis-based methods and optimization-based methods. Analysis-based methods use the statistical information such as vehicle driving conditions, energy and power requirements, and parameters of the battery and UC. Liu *et al.* [7] determined the battery module sizing according to the total energy of the Worldwide harmonized Light-duty vehicles Test Procedure (WLTP) with nominal mileage. The peak power and regenerative energy of the WLTP is assigned to UCs to determine the UC module sizing. The power-energy (PE) function is proposed to obtain the capacity of the HESS with a given load power requirement [8]. Wang *et al.* [9] analyzed the demand power in a random driving cycle and calculated the specific sizing by an improved continuous PE function. However, a potential risk is that the dimensions determined by simple statistical information and computational domain might not meet the requirements of practical applications. Optimization-based

Manuscript received November 30, 2020; revised February 14, 2021; accepted March 27, 2021. Date of publication April 1, 2021; date of current version June 30, 2021. This work was supported by the National Natural Science Foundation of China under Grants 91848111 and 61803359. Recommended for publication by Associate Editor H. Hofmann. *(Corresponding author: Zonghai Chen.)*

The authors are with the Department of Automation, University of Science and Technology of China, Hefei 230052, China (e-mail: limince@mail.ustc.edu.cn; change94@mail.ustc.edu.cn; wangyujie@ustc.edu.cn; chenzh@ustc.edu.cn).

Color versions of one or more figures in this article are available at https://doi.org/10.1109/TPEL.2021.3070393.

Digital Object Identifier 10.1109/TPEL.2021.3070393

methods take economic efficiency, weight limit, and battery lifespan into accounts to obtain the optimal component sizing. Meta-heuristics methods such as particle swarm optimization (PSO) [10] and genetic algorithm (GA) [11] were commonly used for this nonlinear optimization problem. Wu *et al.* [12] used a convex optimization method to obtain the sizing of a fuel cell pack and a battery pack. With determined EMSs, nondominated sorting GA II (NSGA-II) was proposed to obtain the Pareto front (PF) of HESS component sizing by Zhang *et al.* [13] and Eldeeb *et al.* [14]. Although optimization-based methods have greater computational complexity, more suitable sizing solutions can be obtained for the application.

Several EMSs of HESS have been analyzed in the literature, which can be roughly classified into two categories: rule-based strategies (RBSs) and optimization-based strategies (OBSs). RBSs include deterministic RBS [15], fuzzy logic control (FLC) strategy [16], filtering method [17], state machine control [18], etc. Special rules are developed from the logical threshold or frequency domain. RBSs are suitable for online applications with a low computational cost. However, RBSs lack adaption to the complex driving conditions. OBSs obtain optimal power allocation results by maximizing or minimizing the corresponding cost objective function. Model prediction control [9], reinforcement learning [19], game theory [20], and Pontryagin's minimum principle [21] are commonly used for online energy management. As for offline energy management, dynamic programming (DP) can generate the optimal power splitting trajectory between the battery and the UC [22]. Pan *et al.* [23] used DP to minimize the energy loss of the HESS, and the results were better than an RBS. Although DP is not suitable for online applications, it can provide some guidance for EMS. Song *et al.* [24] compared three different topologies using DP, whose cost function involved battery lifespan and energy cost. A near-optimal RBS was extracted from DP results with subjective analysis. Liu *et al.* [7] proposed a three-segment RBS with segment fitting for the relationship between UC power and load power of DP results. The neural networks (NN) method was proposed to conduct online intelligent EMS in Shen and Khaligh [25] and the training datasets were obtained by DP. It is clear from the literature that how to well learn DP results is important for the construction of online EMS.

A new trend of the HESS is the combined optimization of the component sizing and EMS because they are coupled. Yu *et al.* [26] used NSGA-II to obtain Pareto optimal solutions of sizing parameters and membership functions of an online FLC method. Shen *et al.* [27] proposed a sample-based global Dividing RECTangles algorithm to achieve the optimization of sizing and parameters in an RBS. However, EMSs of these two references are not as optimal as DP. The combined or multiobjective optimization method considers both component sizing and parameters in an EMS, so the results are more suitable for practical application.

This article aims to perform the sizing optimization combining with an EMS and apply an adaptive intelligent real-time EMS for practice. Compared with the previous literature, the contributions of this article can be summarized as follows: 1) the Pareto optimal solutions of HESS sizing and parameters in DP objective function are obtained by the multiobjective grey wolf optimizer (MOGWO). In this framework, the HESS cost and battery lifespan are considered as two opposing optimization objectives. 2) Based on the optimal power splitting results of DP with different driving patterns, the random forests (RF) based control mode is constructed and tuned. 3) An adaptive EMS is set up with RF to control power-sharing and support vector machine (SVM) to recognize the current driving pattern. 4) The proposed adaptive RF-based control strategy is verified under a combined load cycle. The performance of the proposed EMS is compared with DP and the ordinary RF-based control method. Results show that the adaptive RF-based EMS is near-optimal to DP.

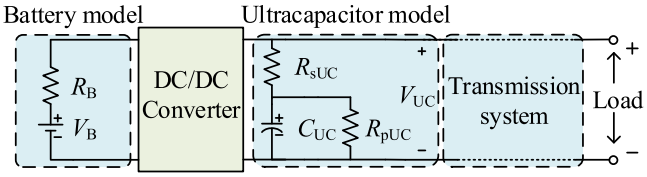

Fig. 1. System topology.

The organization of this article is as follows. In Section II, the system topology and the modeling of each component of HESS are illustrated. Section III presents a multiobjective optimization method to solve the component sizing problem. An online adaptive RF-based EMS is constructed in Section IV. Section V details the verification and evaluation of the proposed strategy with two test cycles, followed by the conclusion Section VI.

II. Modeling for the HESS

The battery semiactive HESS topology is considered in this article.

A. System Topology

The powertrain configuration is sketched in Fig. 1, which is composed of a battery system, an UC system, a dc/dc converter, and a transmission system. The battery system serves as the primary source of energy and is connected to the dc bus via a bidirectional dc/dc converter. The UC system is connected to the dc bus directly so that the UC can be fully utilized. The HESS system is connected to motor load via a transmission system, which involves a dc/ac converter for dc/ac conversion and motor voltage regulation. During the energy management process in DP, the energy efficiency of the dc/dc converter is significant. Therefore, the converter is modeled as a power transfer component with constant efficiency η_{DC} [28].

B. Model of the Vehicle

In this article, only the longitudinal dynamics characteristic is considered. The real-time required power P_{re} can be calculated according to the following:

$$P_{\mathrm{re}} = (\mu M g \cos\theta + M g \sin\theta + 0.5 A \rho_{\mathrm{air}} C_{\mathrm{air}} v^2 + \delta_{\mathrm{c}} M a) v$$

where μ is the rolling resistance coefficient, M is the vehicle mass, g is the gravitational acceleration, θ is the longitudinal

TABLE I
MAIN PARAMETERS OF THE VEHICLE

Parameters	Symbols	Values
Rolling resistance coefficient	μ	0.0015
Vehicle mass	M	1360 kg
Gravitational acceleration	g	9.8 m/s^2
Air density	ρ_{air}	1.202 kg/m^3
Windward area of the vehicle	A	2 m^2
Air resistance coefficient	C_{air}	0.3
Rotation mass correction coefficient	δ_c	1.04
Efficiency of the power transmission system	η_{s}	0.9

TABLE II
MAIN PARAMETERS OF SELECTED BATTERY AND UC

Parameters	Battery	Ultra-capacitor
Nominal voltage	3.7V	2.7V
Nominal capacity	30Ah	–
Nominal capacitance	–	3000F
Energy of cell	111Wh	3.04Wh

road gradient, ρ_{air} is the air density, A is the windward area of the vehicle, C_{air} is the air resistance coefficient, δ_c is the rotation mass correction coefficient, and a is the acceleration.

The parameters of the vehicle are listed in Table I.

Then, the electric drive power P_{e} is formulated as follows:

$$P_{\text{e}} = \begin{cases} P_{\text{re}}/\eta_{\text{s}} & P_{\text{re}} \geq 0 \\ P_{\text{re}} \cdot \eta_{\text{s}} & P_{\text{re}} < 0 \end{cases}$$

where η_{s} is the efficiency of the power transmission system. When P_{re} is positive, the vehicle is in traction mode, and the vehicle is in regenerative braking mode when P_{re} is negative.

C. Model of the Lithium-Ion Battery

A commercial lithium-ion battery is applied in this work, and its main parameters are listed in Table II. The battery dynamic is described by a Rint model, which contains an open-circuit voltage V_{B} and an internal resistance R_{B}. The Rint model is simple and has low computational complexity, so it is suitable for the energy management application at the system level [22]. The battery system consists of N_{sb} cells in series and N_{pb} cells in parallel. The relationship between battery system parameters and cell parameters is determined by the following:

$$Q_{\text{B}} = N_{\text{sb}}N_{\text{pb}}Q_{\text{b}}, R_{\text{B}} = N_{\text{sb}}R_{\text{b}}/N_{\text{pb}}, V_{\text{B}} = N_{\text{sb}}V_{\text{b}}$$

where Q_{B} denotes the nominal capacity of the battery system, R_{b} and V_{b} denote the internal resistance and open-circuit voltage of the battery cell, respectively.

Based on the Rint model, the battery system behavior can be described by the following:

$$I_{\text{B}} = -\frac{V_{\text{B}} - \sqrt{V_{\text{B}}^2 + 4R_{\text{B}}P_{\text{B}}}}{2R_{\text{B}}}$$

where I_{B} denotes the current of the battery system and P_{B} denotes the output power of the battery system.

D. Model of the UC

The Maxwell BCAP3000 UC is applied in this article, and its main parameters are listed in Table II. The UC dynamic is described by a classical model shown in Fig. 1, where R_{sUC} denotes the internal resistance, R_{pUC} denotes the self-discharging resistance, C_{UC} is the equivalent capacitance. The UC system consists of N_{suc} cells in series and N_{puc} cells in parallel. The relationship of UC system parameters and UC cell parameters is determined by the following:

$$\begin{cases} C_{\text{UC}} = N_{\text{puc}}C_{\text{uc}}/N_{\text{suc}}, R_{\text{sUC}} = N_{\text{suc}}R_{\text{suc}}/N_{\text{puc}} \\ R_{\text{pUC}} = N_{\text{suc}}R_{\text{puc}}/N_{\text{puc}}, V_{\text{UC}} = N_{\text{suc}}V_{\text{uc}} \end{cases}$$

where V_{UC} denotes the terminal voltage of the UC system, C_{uc}, R_{suc}, and R_{puc} denote the equivalent capacitance, the internal resistance, and the self-discharging resistance of the UC cell, respectively.

Based on the UC model, the UC system behaviors are expressed as follows:

$$\dot{V}_{\text{pUC}} = I_{\text{UC}}/C_{\text{UC}} - V_{\text{pUC}}/(R_{\text{pUC}}C_{\text{UC}})$$
$$V_{\text{UC}} = V_{\text{pUC}} + I_{\text{UC}}R_{\text{sUC}}$$

where V_{pUC} denotes the voltage of the equivalent capacitance and I_{UC} denotes the current of the UC system.

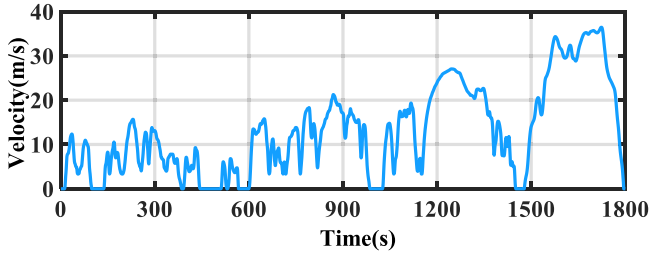

Fig. 2. WLTP driving cycle.

III. SIZING OPTIMIZATION BASED ON MOGWO

Appropriate component sizing is the foundation of an EMS. In this section, the series and parallel number of battery cells is determined by a statistical method. During the multiobjective optimization, the DP algorithm is used as the power distribution strategy. The weights of DP optimization objective function and the series–parallel number of UC cells are optimized simultaneously.

A. Determination of Battery Sizing

The HESS should satisfy both the energy and power requirements during the entire ride of the EV. Of particular note is that energy stored in the UC is much less than that stored in the battery. The main functions of UC are to absorb or release peak power and to deal with high-frequency currents.

In this article, the mileage of nine repeated WLTP is chosen as the nominal mileage, which is 209.2 km. The velocity profile of WLTP is shown in Fig. 2. The required energy for the nominal mileage of the EV is less than the stored energy in the battery system.

The available ranges for the battery are set as 90% depth of discharge. The total number of battery cells can be calculated

according to the following:

$$(1-\eta_{\mathrm{e}})3600U_{\mathrm{b}}Q_{\mathrm{b}}N_{\mathrm{sb}}N_{\mathrm{pb}}\times 90\% \geq 9\int_{t_0}^{t_{\mathrm{end}}} P_{\mathrm{e}}(t)\mathrm{d}t$$

where η_{e} denotes the proportion of power for electronic equipment on the vehicle in the total power, U_{b} denotes the nominal voltage of the battery cell, $P_{\mathrm{e}}(t)$ is calculated according to (1) and (2), and $N_{\mathrm{sb}}, N_{\mathrm{pb}} \in N^*$.

B. DP Based Power Distribution Strategy

In this section, the DP algorithm is utilized to solve the optimal power distribution problem of HESS through offline calculation. The optimal result is specific to a particular optimization objective. In this article, the optimization objective of energy management is set to both reduce the energy loss of the system and extend the lifecycle of the battery system.

The electric drive power P_{e} is completely provided by the battery system and UC system, which can be expressed as as follows:

$$P_{\mathrm{e}} = \begin{cases} P_{\mathrm{UC}} + P_{\mathrm{B}} \cdot \eta_{\mathrm{DC}} & P_{\mathrm{B}} \geq 0 \\ P_{\mathrm{UC}} + P_{\mathrm{B}}/\eta_{\mathrm{DC}} & P_{\mathrm{B}} \leq 0 \end{cases}$$

where P_{UC} and P_{B} denote the power of the UC system and battery system, respectively. The battery system supplies power when P_{B} is positive.

The power loss equations of each component in the battery semiactive HESS topology are formulated as follows:

$$\begin{aligned} P_{\mathrm{loss\_B}} &= I_{\mathrm{B}}^2 R_{\mathrm{B}} \\ P_{\mathrm{loss\_UC}} &= I_{\mathrm{UC}}^2 R_{\mathrm{sUC}} + V_{\mathrm{pUC}}^2/R_{\mathrm{pUC}} \\ P_{\mathrm{loss\_DC}} &= \begin{cases} P_{\mathrm{B}} \cdot (1-\eta_{\mathrm{DC}}) & P_{\mathrm{B}} \geq 0 \\ P_{\mathrm{B}}/(1-\eta_{\mathrm{DC}}) & P_{\mathrm{B}} \leq 0. \end{cases} \end{aligned}$$

In the EV application, the battery is regarded as the end of the lifecycle when the capacity reaches 80% of the rated capacity [29]. The Ah-throughput is a crucial factor for the capacity fading of the battery [7]. A widely used semiempirical lifecycle model is expressed as as follows [30]:

$$Q_{\mathrm{loss}} = B \cdot \exp\left(\frac{-E_{\mathrm{a}}}{RT}\right)(A_{\mathrm{h}})^z$$

where B is the preexponential factor, E_{a} is the activation energy in J/mol, R is the gas constant, T is the absolute temperature, A_{h} is the Ah-throughput, and z is the power-law factor.

In this work, the total Ah-throughput during the EV driving cycle is another objective to minimize during the power distribution by DP, which is formulated as as follows:

$$A_{\mathrm{h}} = \frac{1}{3600}\int_{t_0}^{t_{\mathrm{end}}} |I_{\mathrm{B}}|\mathrm{d}t.$$

Through the above analysis, the objective function of the DP is defined as follows:

$$\min J = \min(\omega_1 E_{\mathrm{loss\_B}} + \omega_2 E_{\mathrm{loss\_UC}} + \omega_3 E_{\mathrm{loss\_DC}} + \omega_4 A_{\mathrm{h}})$$
$$\text{s.t.} \begin{cases} I_{\mathrm{Bmin}} \leq I_{\mathrm{B}} \leq I_{\mathrm{Bmax}} \\ I_{\mathrm{UCmin}} \leq I_{\mathrm{UC}} \leq I_{\mathrm{UCmax}} \\ \mathrm{SOC}_{\mathrm{Bmin}} \leq \mathrm{SOC}_{\mathrm{B}} \leq \mathrm{SOC}_{\mathrm{Bmax}} \\ \mathrm{SOV}_{\mathrm{UCmin}} \leq \mathrm{SOV}_{\mathrm{UC}} \leq \mathrm{SOV}_{\mathrm{UCmax}} \\ \mathrm{SOV}_{\mathrm{UC\_}t_0} = \mathrm{SOV}_{\mathrm{UC\_}t_{\mathrm{end}}} \end{cases}$$

where ω_1, ω_2, ω_3, and ω_4 are four weights determined by multiobjective optimization, which will be introduced in next section, $E_{\mathrm{loss\_B}}$, $E_{\mathrm{loss\_UC}}$, and $E_{\mathrm{loss\_DC}}$ denote the energy loss of battery system, UC system, and dc–dc converter, respectively, $\mathrm{SOC_B}$ denotes the state-of-charge (SOC) of the battery system, $\mathrm{SOV_{UC}}$ denotes the state-of-voltage (SOV) of UC system.

The SOC of the battery is calculated using Ampere–hour integral method [31]. The SOV of the UC system is defined as follows:

$$\mathrm{SOV_{UC}} = (V_{\mathrm{UC}} - V_{\mathrm{UCmin}})/(V_{\mathrm{UCmax}} - V_{\mathrm{UCmin}})$$

where V_{UCmin} and V_{UCmax} denote the lower and upper voltage limits of the UC system. For an UC cell, V_{ucmin} and V_{ucmax} are 1.35 and 2.7 V, respectively.

The voltage of the UC system is selected as the unique control variable. The initial and final values of V_{UC} are both set as the median value as the voltage range of the UC system. This aims to keep the long-term functioning ability of the UC system.

In the path planning process of the DP algorithm, V_{UC} is discretized to 1000 different states with uniform distribution in the whole decision space. The complexity of DP is exponentially related to the number of search variables. During the entire driving cycle, the battery system voltage variation is much smaller than UC system. To simplify the calculation, the voltage of the battery cell is treated as a constant of 3.7 V, which is a common assumption in the DP search process [7] [32]. The effect of the state of health on parameters of battery and UC models is also neglected.

C. Multiobjective Optimization Using MOGWO

The sizing of the battery system is determined via an analysis-based method, while the number of UC cells in series N_{suc} and in parallel N_{puc} remains unsolved. The two parameters of component sizing and four weights of the DP objective function are optimized simultaneously in this section.

1) Description of Sizing Optimization: These six optimal values should minimize the cost of the HESS system, and maximize the remaining cycle life of the battery system. From the financial perspective, the cost of the battery system and dc/dc converter can be seen as a constant. The cost of the UC system is listed as the financial optimization objective. The other objective is to minimize the Ah-throughput of the battery system for the WLTP driving cycle. It can be seen from (13) that minimizing A_{h} is equivalent to minimizing the capacity fade of battery when other parameters keep the same. The objective function of sizing

optimization is formulated as follows:

$$\min O = \min \begin{cases} o_1 = c_{\text{uc}} N_{\text{suc}} N_{\text{puc}} \\ o_2 = A_{\text{h}}(\omega_1, \omega_2, \omega_3, \omega_4, N_{\text{suc}}, N_{\text{puc}}) \end{cases}$$
$$\text{s.t.} \begin{cases} N_{\text{suc}}, N_{\text{puc}} \in N^* \\ 35 \le N_{\text{suc}} \le 79 \\ 1 \le N_{\text{puc}} \le 5 \\ 0.1 \le \omega_1, \omega_2, \omega_3, \omega_4 \le 50 \end{cases}$$

where c_{uc} denotes the cost of the UC cell, the range of N_{suc} is determined by the voltage range of the dc/dc converter. The duty cycle of the buck dc/dc converter is determined as $[25\%, 85\%]$ to ensure life duration and efficiency. N_{puc} should be chosen in a relatively small quantitative range.

2) Description of MOGWO: The MOGWO [33] is utilized to solve the sizing optimization problem of HESS. The Grey Wolf Optimizer (GWO) is one of the most recent swarm intelligent techniques, which mimics the hierarchy and hunting behavior of grey wolfs. The wolves are divided into four classes: alpha (α), beta (β), delta (δ), and omega (ω). In MOGWO, α, β, δ are three solutions in the PF to mimic the power hierarchy of wolves in nature. The rest of the solutions are considered as ω, whose position values are updated according to the values of α, β, and δ. Mathematical expressions are formulated as follows:

$$\mathbf{D}_\alpha = C_1 \mathbf{X}_\alpha - \mathbf{X}, \mathbf{D}_\beta = C_2 \mathbf{X}_\beta - \mathbf{X}, \mathbf{D}_\delta = C_3 \mathbf{X}_\delta - \mathbf{X}$$
$$\mathbf{X}_1 = \mathbf{X}_\alpha - H_1 \mathbf{D}_\alpha, \mathbf{X}_2 = \mathbf{X}_\beta - H_2 \mathbf{D}_\beta, \mathbf{X}_3 = \mathbf{X}_\delta - H_3 \mathbf{D}_\delta$$
$$\mathbf{X}(t+1) = (\mathbf{X}_1 + \mathbf{X}_2 + \mathbf{X}_3)/3$$

where $\mathbf{X}$ denotes the position vector of a single wolf, $\mathbf{X}_\alpha$, $\mathbf{X}_\beta$, and $\mathbf{X}_\delta$ denotes the position vector of α, β, and δ, respectively, and C and H are two coefficients in GWO.

During each iteration, C and H are updated according to the following:

$$\begin{cases} \lambda(k) = 2 - 2\,k/K \\ C = 2r_1 \\ H = 2\lambda(k) r_2 - \lambda(k) \end{cases}$$

where k is the number of iteration, K denotes the maximum number of iterations, r_1 and r_2 are two random numbers in the range [0,1].

In this article, $\mathbf{X}$ is formulated as follows:

$$\mathbf{X} = (\omega_1, \omega_2, \omega_3, \omega_4, N_{\text{suc}}, N_{\text{puc}}).$$

After the optimization, the nondominated solutions are expressed as the PF. The leader selection method to choose α, β, δ is roulette wheel selection. Solutions in the most crowded segment have the least probability to be leaders. The framework of sizing optimization using MOGWO is shown in Fig. 3.

D. Results of Sizing Optimization

The population size of MOGWO is set as 100, and the maximum number of iterations is set as 100. The number of battery cells is more than 288 according to (8). The series number of battery cells is determined by the dc link voltage. In this work, N_{sb} is chosen as 58 and N_{pb} is chosen as 5.

The PF of sizing optimization is shown in Fig. 4. Every solution of the PF is optimal to some extent. The special solution can be chosen by manufacturers considering the tradeoff between cost and battery remaining lifecycle. In this article, the technique for order preference by similarity to an ideal solution method is adopted to obtain the most preferable solution [34]. Therefore, the optimal component sizing is determined as $N_{\text{sb}} = 58$, $N_{\text{pb}} = 5$, $N_{\text{suc}} = 44$, $N_{\text{puc}} = 1$, and is shown as the blue point in Fig. 4.

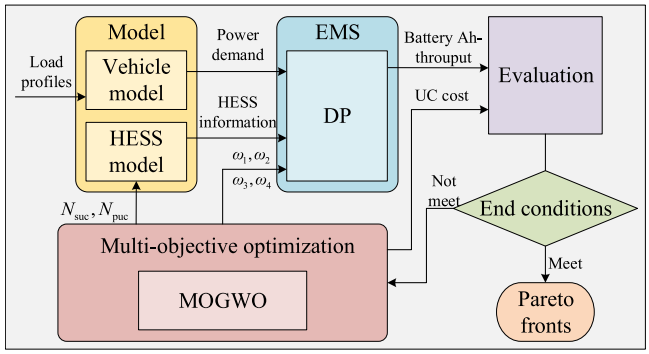

Fig. 3. Framework of sizing optimization using MOGWO.

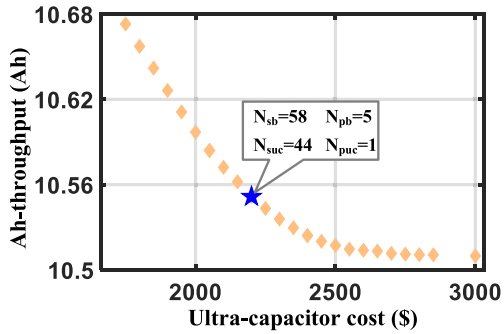

Fig. 4. PF of WLTP.

IV. Online EMS

When the component sizing of HESS is determined, the optimal power-splitting trajectory can be obtained using the DP algorithm. However, the offline calculation cannot be applied directly to a practical situation. RF, as a high-precision machine learning method with strong interpretability, is used to extract the rules from the DP results in this article.

A. Framework

The proposed optimization design, management, and control framework is presented in Fig. 5. The combined methods are divided into three main parts: offline sizing optimization, offline training of RF and SVM, and online EMS implementation.

The sizing optimization method based on MOGWO has been given in Section III. In the bilevel sizing optimization strategy, DP is the inner loop EMS and MOGWO is the outer loop sizing optimization algorithm. The offline bilevel sizing optimization results give the optimal sizing parameters of HESS and optimal weights of DP, which are the foundation for the creation of the EMS dataset.

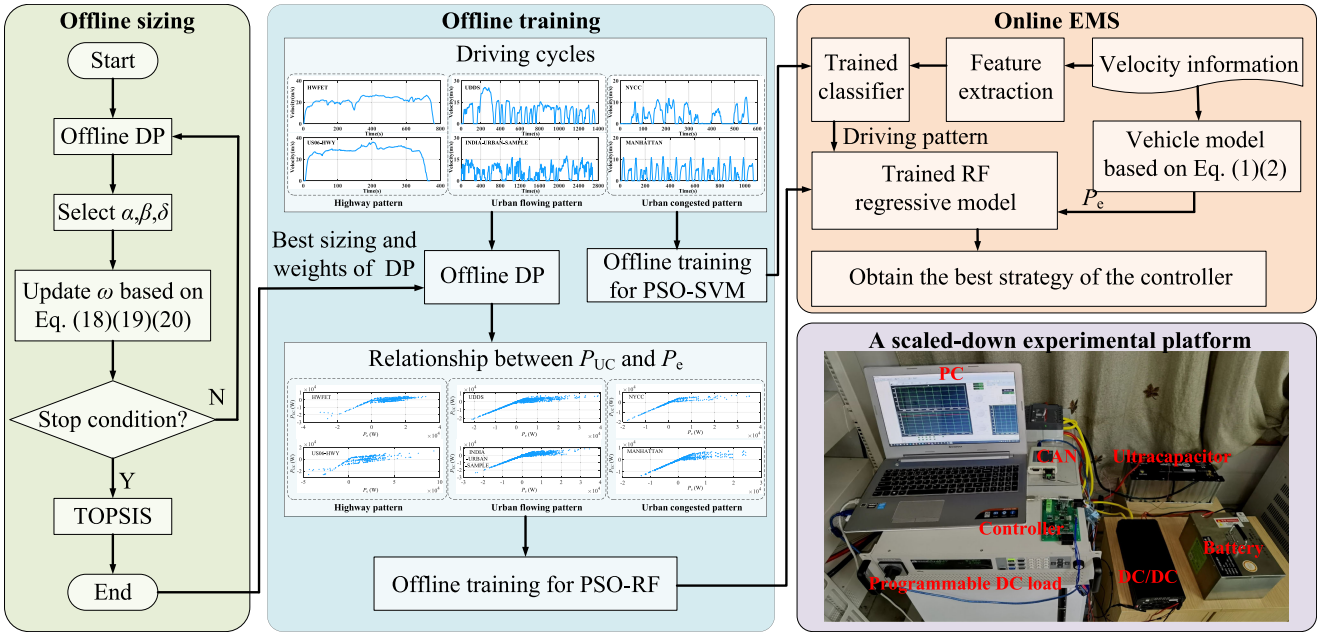

Fig. 5. Framework of control strategy.

In the offline EMS training stage, three driving patterns are considered. On the one hand, optimal energy management results can be obtained using DP with sizing and weights from sizing optimization part. The relationship between UC system power and electric drive power is extracted as the EMS dataset to train PSO-RF. On the other hand, four speed features of different driving patterns are extracted to train SVM.

The online EMS is composed of two parts: the trained RF regressive model and the trained SVM classification model. In the online EMS implementation stage, the driving pattern is recognized by the trained classifier with feature extraction. The driving pattern and P_e calculated by (1) and (2) are the inputs of the trained regressive model, while the output of the RF is the P_{UC}. Then, the specific control variables I_B, V_{UC}, and I_{UC} can be calculated based on the HESS system model.

The specific details of offline EMS training and online EMS implementation will be presented in the following sections.

B. Analysis of DP Results

To better understand the regular laws of the optimal DP results, six different driving cycles are considered and analyzed to develop the common rules. From Fig. 5, it is obvious that six standard driving cycles belong to three different driving patterns, which are highway pattern (HWFET, US06-HWY), urban flowing pattern (UDDS, INDIA-URBAN-SAMPLE), and urban congested pattern (NYCC, MANHATTAN).

The optimal power allocation results are shown in Fig. 6. It can be seen that almost all the regenerative power is absorbed by the UC system, and peak positive power is shared between the battery system and the UC system. The battery system charges the UC system sometimes. A possible explanation for this result might be that the UC system should keep the same SOV between

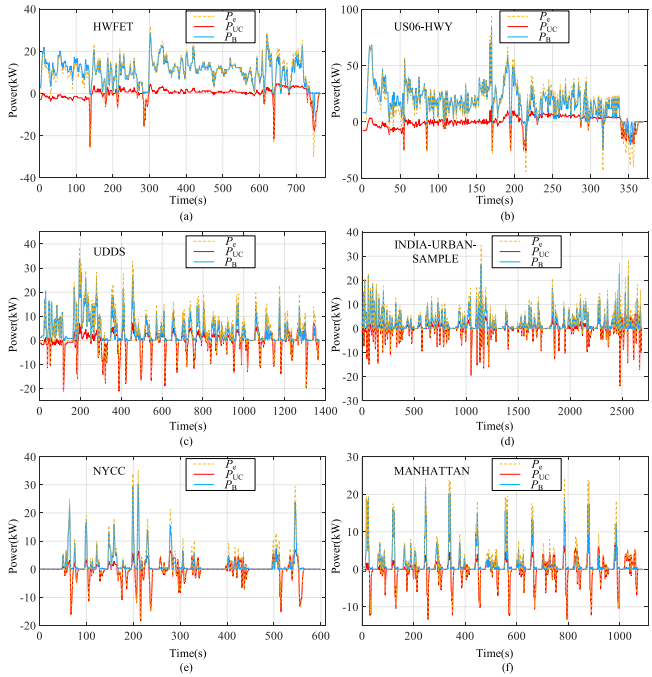

Fig. 6. DP results of different driving cycles. (a) HWFET; (b) US06-HWY; (c) UDDS; (d) INDIA-URBAN-SAMPLE; (e) NYCC; (f) MANHATTAN.

the initial and final state of a whole driving cycle as mentioned in (15).

The power splitting results are not clear enough to extract some general rules for online applications. The relationship of UC system power and electric drive power is sketched in Fig. 7 for further analysis. Although six different driving cycles are conducted, the UC behaviors are similar. There is some explicit relationship between P_{UC} and P_e. Liu *et al.* [7] proposed a piecewise linearization strategy to describe this relationship.

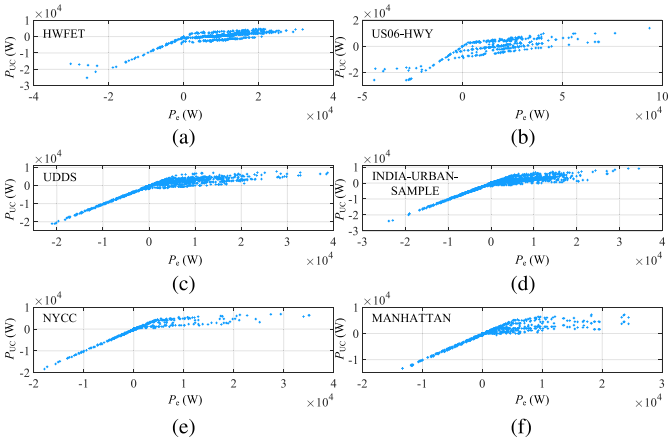

Fig. 7. Relationship between P_e and P_{UC}. (a) HWFET; (b) US06-HWY; (c) UDDS; (d) INDIA-URBAN-SAMPLE; (e) NYCC; (f) MANHATTAN.

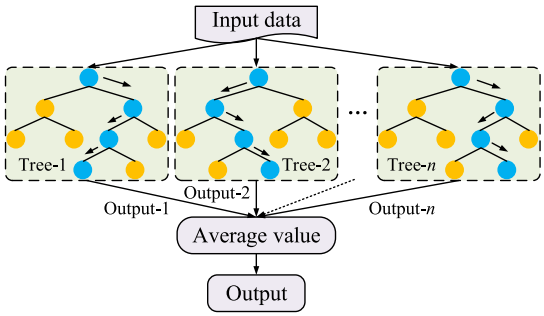

Fig. 8. Schematic of RF.

However, this method of extracting rules is not intelligent enough compared with machine learning methods and some nonlinear factors are ignored. This article proposes a novel method, which utilizes the RF algorithm to extract the rules from DP results.

C. Construction of RF Regression Model

RF regression is an ensemble learning method proposed by Breiman [35], which is composed of a multitude of decision trees. The training data of every single tree is extracted from the original training set via a bootstrap sample and the sample size is the same. As shown in Fig. 8, once the RF regression model is constructed, each decision tree processes input data by comparing the numerical value and the threshold value of each node. Notice that the threshold value of each node is formed through the training process. If the input data satisfies the judging condition, it moves on that branch until it reaches a leaf node. The final output is represented as the mean output value of all single trees. The randomness of the bootstrap sample and threshold formation makes the model less susceptible to overfitting and robust to external noise.

In this article, P_e is chosen as the only one input. Accordingly, P_{UC} can be output through the regression mapping relationship constructed by the RF model. The training data for the RF model comes from the optimal power splitting results obtained through the DP method. The data from two driving cycles of the same driving mode are blended to highlight differences in driving patterns. To generate the RF regression model, 80% of the dataset is taken for training and 20% is for testing.

There are three main hyperparameters of the RF model: 1) the number of trees in the forest n_{tree}; 2) the number of features considered in each tree $n_{feature}$; 3) the minimum number of nodes in the decision tree $n_{nodesize}$. Since the value of P_e is the only input feature, the second hyperparameter is fixed to one. The PSO method [36] is adopted to achieve parameter tuning. The best parameters are selected with the least mean square error of the five-fold cross-validation [37]. The specific PSO-RF algorithm is described in Table III.

The boundary constraints of the two hyperparameters are as follows: $n_{tree} \in [10, 1000]$, $n_{nodesize} \in [2, 50]$. With the help of the PSO algorithm, the optimal values for different driving patterns are determined and given in Table IV.

TABLE III
PSO-RF ALGORITHM

Step 1	Initialization. (a). Determine the boundary of n_{tree} and $n_{nodesize}$; (b). Determine the internal parameters of PSO, such as c_1, c_2, the maximum number of iteration K, population size I; (c). Generate position and velocity vector of each particle randomly; (d). Initialize individual best position P_{ibest} and global best position P_{gbest}. (e). Initialize the number of iterations k and the number of particles i: $k = 1$, $i = 1$.
Step 2	Updating. (a). Update position and velocity of each particle: $\begin{cases} v_i^{k+1} = v_i^k + c_1 r_1 (P_{ibest} - x_i^k) + c_2 r_2 (P_{gbest} - x_i^k) \\ x_i^{k+1} = x_i^k + v_i^{k+1} \end{cases}$ where r_1 and r_2 are two random numbers between 0 and 1. (b). Update individual and global best position: $P_{ibest} = \begin{cases} x_i^{k+1} & \text{if } F(x_i^{k+1}) < F(P_{ibest}) \\ P_{ibest} & \text{if } F(x_i^{k+1}) \geq F(P_{ibest}) \end{cases}$ $P_{gbest} = \begin{cases} x_i^{k+1} & \text{if } F(x_i^{k+1}) < F(P_{gbest}) \\ P_{gbest} & \text{if } F(x_i^{k+1}) \geq F(P_{gbest}) \end{cases}$ (c). Update the number of particle: $i = i + 1$.
Step 3	Judging. (a). If $i \leq I$, jump to Step 2. (b). If $i > I$, and $k < K$, jump to Step 2 and $k = k + 1$. (c). If $k = K$, save the optimal solution of n_{tree} and $n_{nodesize}$, and go to Step 4.
Step 4	RF training. Obtain the RF regression model using tuned parameters.

TABLE IV
OPTIMAL VALUES OF HYPERPARAMETERS

RF hyper-parameters	Boundary constraints	Optimal values		
		Highway	Urban flowing	Urban congested
n_{tree}	[10,1000]	111	383	155
$n_{nodesize}$	[2,50]	27	25	28

D. Driving Condition Recognition

Since the RF regression model is built with prior knowledge of the determining driving patterns, driving pattern recognition (DPR) is required for real-time application with RF models. As the speed can be obtained online, four speed statistical features representing different driving modes are extracted: average speed, maximum and minimum acceleration, and idle time in the

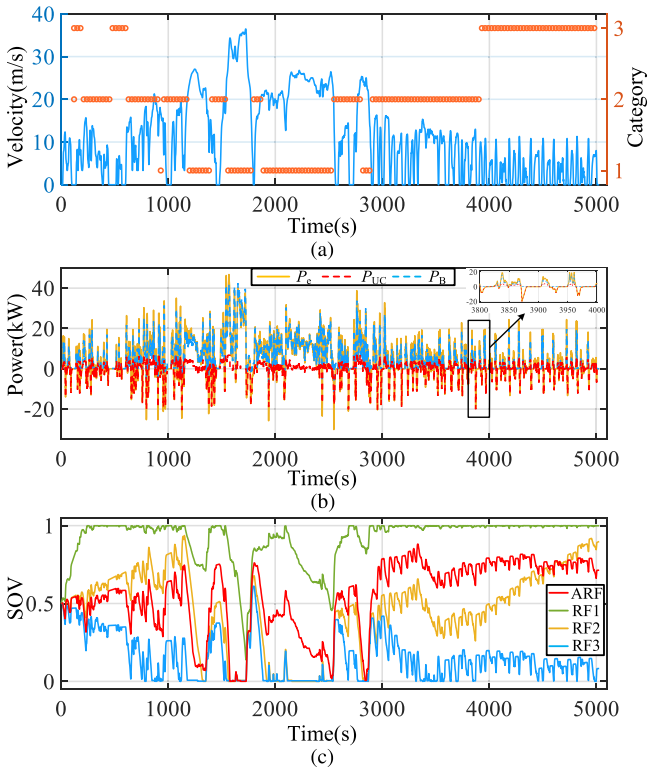

Fig. 9. Results in the combined load cycle. (a) Velocity and DPR results. (b) Power splitting results of ARF. (c) SOV of UC system.

last 120 s. In this article, SVM is utilized to realize the DPR and the specific process is referred to Ref. [21].

V. Verification

In this article, the parameters of the battery and UC cell model are identified using the recursive least-squares method [38]. To verify the proposed intelligent real-time EMS using the RF regression model, a combined dynamic driving condition is carried out. This combined load cycle includes WLTP, HWFET, UDDS, and MANHATTAN driving cycle connected back to back. Five power distribution strategies are compared. The proposed adaptive RF (ARF) based control strategy is first carried out. The ARF contains a SVM model to recognize the driving pattern and a RF model to predict the UC system power. The second, third, and fourth cases are the RF-based control strategies without DPR, namely RF1, RF2, and RF3, whose parameters are tuned under HWFET, UDDS, and MANHATTAN driving cycle, respectively. The last strategy is DP with offline calculation, which knows the full test driving cycle. DP can obtain the optimal energy management results, but DP is an offline method. For DP, all the driving profiles should be given at the beginning of optimization calculation process. However, in the real-world application, the information about the future working conditions is unknown. So, DP is usually treated as one of the benchmarks for comparison.

The detailed power distribution results are shown in Fig. 9. Fig. 9(a) shows the DPR results, where category 1 is highway pattern, category 2 is urban flowing pattern, and category 3 is urban congested pattern. From the results, it can be seen that the trained SVM model can perform the task of DPR well. Then, the corresponding RF regression model is selected according the DPR result in ARF method. The results of the power distribution of the ARF method are given in Fig. 9(b). It can be seen from Fig. 9(b) that the UC system absorbs the regenerative braking power well and limits the peak battery discharge power. Fig. 9(c) shows the UC system SOV trajectories under different cases. Results show that ARF makes UC better performance than RF without DPR. In RF1, UC reaches the maximum value of voltage limits early and hard to absorb more regenerative braking power. In RF3, UC reaches the minimum value of voltage limits early, and hard to share the peak discharge power. The performance of RF2 is similar to that of ARF, but ARF reaches the voltage limits less frequently and the final value of V_{UC} is closer to the initial value. Therefore, the RF-based control strategies whose parameters are trained by a single driving pattern lacks adaptability and the overall performance is not as good as the ARF algorithm. There is one notable place in the results. In Fig. 9(b), the UC system helps the battery to take up some of the power at around 1500 s. At around 1600 s, the UC system voltage reaches the lower bound, as seen in Fig. 9(c), so it cannot continue to help share the energy. The size of the UC system is determined in Section III using a multiobjective optimization method. From the point of view of system cost, the number of UC cells will not be too large. So, it is inevitable that a situation like around 1600 s will occur.

To evaluate the performance of the battery system, the root-mean-square current of the battery system (I_{RMS}), the peak discharge and charge current (I_{pd} and I_{pc}), and the Ah-throughout of the battery system (A_h) are compared in Table V. Compared with ordinary RF, I_{RMS} is reduced by 2.01%–8.93%, A_h is reduced by 0.5%–19.83%, I_{pd} is reduced by 6.15%–13.32%, and I_{pc} is reduced by 3.13%–48.07%. Compared with DP, I_{RMS}, A_h, and I_{pd} are reduced by 3.37%, 1.37%, and 12.9%, respectively. ARF has the optimal performance in protecting battery from large current spikes and power shocks.

Since the RF is used to extract rules from DP, the objective function value (J) of DP in (15) is also compared. DP obtains the optimal result and ARF obtains the near-optimal J value, proving the superiority of ARF. To evaluate the performance of energy efficiency, the energy loss of battery system (L_1), dc/dc converter (L_2), UC system (L_3), and total system (L_0) are compared in Table V. ARF achieves minimal battery energy loss. Compared with ordinary RF and DP, the battery energy loss is reduced by 4.15%–20.58%. Compared with ordinary RF, the total energy loss is reduced by 0.74%–9.49%. In terms of energy efficiency, ARF achieves a near-optimal result, second only to DP and better than ordinary RF methods.

In conclusion, the DP method has the optimal results obtained by offline calculation for the objective function value J. The proposed ARF-based EMS has the best overall performance, considering the performance of the UC system, battery system, and energy efficiency. ARF allows the UC system to fully stretch its role and thus protects the battery. In a comprehensive view, the ARF algorithm proposed in this article is applicable to online energy management.

TABLE V
COMPARISON OF FIVE EMSS UNDER COMBINED LOAD CYCLE

EMS	J	L_1(Wh)	L_2(Wh)	L_3(Wh)	L_0(Wh)	I_{RMS}(A)	A_{h}(Ah)	I_{pd} (A)	I_{pc} (A)
ARF	4.9963×10^7	**121.9743**	380.5081	166.9465	669.4289	**41.3732**	**34.8870**	**188.9912**	-59.7221
RF1	6.2431×10^7	147.0778	476.1838	**51.1430**	674.4047	45.4316	43.5187	201.3677	-114.9946
RF2	5.0273×10^7	127.0370	382.6321	170.6878	680.3569	42.2231	35.0618	218.0209	-61.6511
RF3	5.1321×10^7	134.2006	390.2580	215.1585	739.6171	43.3972	35.7208	218.0209	-83.1365
DP	$\mathbf{4.9028\times10^7}$	130.3395	**372.9463**	120.1935	**623.4793**	42.7684	35.3635	213.3516	**-31.2253**

VI. CONCLUSION

This article has conducted a multiobjective optimization for HESS dimensioning and weights of DP and has applied an adaptive RF-based EMS for application. The series–parallel number of UC cells and four weights of internal EMS using DP have been optimized simultaneously to minimize system cost and battery Ah-throughput based on MOGWO. With optimal parameters, DP results of different driving patterns have been analyzed. The RF method has been proposed to extract the relationship between P_{e} and P_{UC}. DPR has been realized using SVM. The ARF-based EMS, which is composed of RF to conduct power splitting strategy and SVM to identify the driving pattern, has been verified with a combined load cycle. Compared with ordinary RF-based EMS, the total energy loss has been reduced by 0.74%–9.49%, and the battery Ah-throughput has been reduced by 0.5%–19.83%. The performance of the proposed method has achieved less battery root-mean-square current, Ah-throughput, and peak discharge current than DP. Results show that ARF has the optimal overall performance in UC utilization, battery protecting, and energy efficiency.

Our future work is to develop a reinforcement learning based EMS, which will take into account both UC aging and battery aging.

REFERENCES

[1] J. Baars, T. Domenech, R. Bleischwitz, H. E. Melin, and O. Heidrich, "Circular economy strategies for electric vehicle batteries reduce reliance on raw materials," *Nat. Sustain.*, vol. 4, no. 1, pp. 71–79, 2021.

[2] R. Xiong, H. Chen, C. Wang, and F. Sun, "Towards a smarter hybrid energy storage system based on battery and ultracapacitor-a critical review on topology and energy management," *J. Cleaner Prod.*, vol. 202, pp. 1228–1240, 2018.

[3] Y. Wang, C. Liu, R. Pan, and Z. Chen, "Modeling and state-of-charge prediction of lithium-ion battery and ultracapacitor hybrids with a co-estimator," *Energy*, vol. 121, pp. 739–750, 2017.

[4] Y. Wang, M. Li, and Z. Chen, "Experimental study of fractional-order models for lithium-ion battery and ultra-capacitor: Modeling, system identification, and validation," *Appl. Energy*, vol. 278, 2020, Art. no. 115736.

[5] Y. Wang, L. Wang, M. Li, and Z. Chen, "A review of key issues for control and management in battery and ultra-capacitor hybrid energy storage systems," *eTransportation*, vol. 4, 2020, Art. no. 100064.

[6] J. Cao and A. Emadi, "A new battery/ultracapacitor hybrid energy storage system for electric, hybrid, and plug-in hybrid electric vehicles," *IEEE Trans. Power Electron.*, vol. 27, no. 1, pp. 122–132, Jan. 2012.

[7] C. Liu, Y. Wang, L. Wang, and Z. Chen, "Load-adaptive real-time energy management strategy for battery/ultracapacitor hybrid energy storage system using dynamic programming optimization," *J. Power Sour.*, vol. 438, 2019, Art. no. 227024.

[8] Q. Xiaodong, W. Qingnian, and Y. YuanBin, "Power demand analysis and performance estimation for active-combination energy storage system used in hybrid electric vehicles," *IEEE Trans. Veh. Technol.*, vol. 63, no. 7, pp. 3128–3136, Sep. 2014.

[9] L. Wang, Y. Wang, C. Liu, D. Yang, and Z. Chen, "A power distribution strategy for hybrid energy storage system using adaptive model predictive control," *IEEE Trans. Power Electron.*, vol. 35, no. 6, pp. 5897–5906, Jun. 2019.

[10] A. Ostadi and M. Kazerani, "A comparative analysis of optimal sizing of battery-only, ultracapacitor-only, and battery-ultracapacitor hybrid energy storage systems for a city bus," *IEEE Trans. Veh. Technol.*, vol. 64, no. 10, pp. 4449–4460, Oct. 2015.

[11] M. Masih-Tehrani, M.-R. Ha'iri-Yazdi, V. Esfahanian, and A. Safaei, "Optimum sizing and optimum energy management of a hybrid energy storage system for lithium battery life improvement," *J. Power Sources*, vol. 244, pp. 2–10, 2013.

[12] X. Wu, X. Hu, X. Yin, L. Li, Z. Zeng, and V. Pickert, "Convex programming energy management and components sizing of a plug-in fuel cell urban logistics vehicle," *J. Power Sources*, vol. 423, pp. 358–366, 2019.

[13] L. Zhang, X. Hu, Z. Wang, F. Sun, J. Deng, and D. G. Dorrell, "Multiobjective optimal sizing of hybrid energy storage system for electric vehicles," *IEEE Trans. Veh. Technol.*, vol. 67, no. 2, pp. 1027–1035, Feb. 2018.

[14] H. H. Eldeeb, A. T. Elsayed, C. R. Lashway, and O. Mohammed, "Hybrid energy storage sizing and power splitting optimization for plug-in electric vehicles," *IEEE Trans. Ind. Appl.*, vol. 55, no. 3, pp. 2252–2262, May 2019.

[15] O. Veneri, C. Capasso, and S. Patalano, "Experimental investigation into the effectiveness of a super-capacitor based hybrid energy storage system for urban commercial vehicles," *Appl. Energy*, vol. 227, pp. 312–323, 2018.

[16] Q. Zhang and G. Li, "Experimental study on a semi-active battery-supercapacitor hybrid energy storage system for electric vehicle application," *IEEE Trans. Power Electron.*, vol. 35, no. 1, pp. 1014–1021, Jan. 2020.

[17] Q. Zhang, F. Ju, S. Zhang, W. Deng, J. Wu, and C. Gao, "Power management for hybrid energy storage system of electric vehicles considering inaccurate terrain information," *IEEE Trans. Automat. Sci. Eng.*, vol. 14, no. 2, pp. 608–618, Apr. 2017.

[18] Q. Li *et al.*, "A state machine control based on equivalent consumption minimization for fuel cell/supercapacitor hybrid tramway," *IEEE Trans. Transport. Electrific.*, vol. 5, no. 2, pp. 552–564, Jun. 2019.

[19] R. Xiong, J. Cao, and Q. Yu, "Reinforcement learning-based real-time power management for hybrid energy storage system in the plug-in hybrid electric vehicle," *Appl. energy*, vol. 211, pp. 538–548, 2018.

[20] Z. Sun, Y. Wang, Z. Chen, and X. Li, "Min-max game based energy management strategy for fuel cell/supercapacitor hybrid electric vehicles," *Appl. Energy*, vol. 267, 2020, Art. no. 115086.

[21] X. Li, Y. Wang, D. Yang, and Z. Chen, "Adaptive energy management strategy for fuel cell/battery hybrid vehicles using pontryagin's minimal principle," *J. Power Sources*, vol. 440, 2019, Art. no. 227105.

[22] X. Lu and H. Wang, "Optimal sizing and energy management for cost-effective pev hybrid energy storage systems," *IEEE Trans. Ind. Informat.*, vol. 16, no. 5, pp. 3407–3416, May 2020.

[23] C. Pan, Y. Liang, L. Chen, and L. Chen, "Optimal control for hybrid energy storage electric vehicle to achieve energy saving using dynamic programming approach," *Energies*, vol. 12, no. 4, 2019, Art. no. 588.

[24] Z. Song, H. Hofmann, J. Li, X. Han, X. Zhang, and M. Ouyang, "A comparison study of different semi-active hybrid energy storage system topologies for electric vehicles," *J. Power Sources*, vol. 274, pp. 400–411, 2015.

[25] J. Shen and A. Khaligh, "A supervisory energy management control strategy in a battery/ultracapacitor hybrid energy storage system," *IEEE Trans. Transport. Electrific.*, vol. 1, no. 3, pp. 223–231, Oct. 2015.

[26] H. Yu, F. Castelli Dezza, F. Cheli, X. Tang, X. Hu, and X. Lin, "Dimensioning and power management of hybrid energy storage systems for electric vehicles with multiple optimization criteria," *IEEE Trans. Power Electron.*, vol. 36, no. 5, pp. 5545–5556, May 2021.

[27] J. Shen, S. Dusmez, and A. Khaligh, "Optimization of sizing and battery cycle life in battery/ultracapacitor hybrid energy storage systems for electric vehicle applications," *IEEE Trans. Ind. Informat.*, vol. 10, no. 4, pp. 2112–2121, Nov. 2014.
[28] Z. Huang *et al.*, "Modeling and multi-objective optimization of a stand-alone PV-hydrogen-retired EV battery hybrid energy system," *Energy Convers. Manage.*, vol. 181, pp. 80–92, 2019.
[29] R. Xiong, Y. Pan, W. Shen, H. Li, and F. Sun, "Lithium-ion battery aging mechanisms and diagnosis method for automotive applications: Recent advances and perspectives," *Renew. Sustain. Energy Rev.*, vol. 131, 2020, Art. no. 110048.
[30] J. Wang *et al.*, "Cycle-life model for graphite-lifepo4 cells," *J. Power Sources*, vol. 196, no. 8, pp. 3942–3948, 2011.
[31] Y. Wang *et al.*, "A comprehensive review of battery modeling and state estimation approaches for advanced battery management systems," *Renew. Sustain. Energy Rev.*, vol. 131, 2020, Art. no. 110015.
[32] Z. Song, H. Hofmann, J. Li, X. Han, and M. Ouyang, "Optimization for a hybrid energy storage system in electric vehicles using dynamic programing approach," *Appl. Energy*, vol. 139, pp. 151–162, 2015.
[33] S. Mirjalili, S. Saremi, S. M. Mirjalili, and L. d. S. Coelho, "Multi-objective grey wolf optimizer: A novel algorithm for multi-criterion optimization," *Expert Syst. Appl.*, vol. 47, pp. 106–119, 2016.
[34] Y.-J. Lai, T.-Y. Liu, and C.-L. Hwang, "Topsis for MODM," *Eur. J. Oper. Res.*, vol. 76, no. 3, pp. 486–500, 1994.
[35] L. Breiman, "Random forests," *Mach. Learn.*, vol. 45, no. 1, pp. 5–32, 2001.
[36] J. Kennedy and R. Eberhart, "Particle swarm optimization," in *Proc. IEEE ICNN'95-Int. Conf. Neural Netw.*, vol. 4, 1995, pp. 1942–1948.
[37] J. D. Rodriguez, A. Perez, and J. A. Lozano, "Sensitivity analysis of k-fold cross validation in prediction error estimation," *IEEE Trans. Pattern Anal. Mach. Intell.*, vol. 32, no. 3, pp. 569–575, Mar. 2010.
[38] Y. Wang, X. Zhang, C. Liu, R. Pan, and Z. Chen, "Multi-timescale power and energy assessment of lithium-ion battery and supercapacitor hybrid system using extended kalman filter," *J. Power Sources*, vol. 389, pp. 93–105, 2018.

Mince Li (Student Member, IEEE) was born in 1997. He received the B.Sc. degree in electrical engineering from Beijing Jiaotong University, Beijing, China, in 2019. He is currently working toward the M.Sc. degree in control science and engineering with the University of Science and Technology of China, Hefei, China.

His research interests include modeling and control for complex systems, state estimation, energy management and sizing optimization for HESS.

Li Wang (Student Member, IEEE) was born in 1994. She received the B.Sc. degree in automation engineering from Central South University, Changsha, China, in 2017. She is currently working toward the Ph.D. degree in control science and engineering with the University of Science and Technology of China, .

Her research interests include complex system modeling and control, such as state estimation, model predictive control and energy management for hybrid battery/supercapacitor system.

Yujie Wang (Member, IEEE) received the Ph.D. degree in control science and engineering from the University of Science and Technology of China, Hefei, China, in 2017.

He was a Postdoctoral Researcher and is currently an Associate Research Fellow with the Department of Automation, University of Science and Technology of China. His research interests include management of energy storage system, new energy vehicle technology, complex system modeling, simulation and control, fuel cell system management and optimization control.

Dr. Wang was a recipient of the Excellent Doctoral Dissertation and Special Award of President of the Chinese Academy of Sciences, and the Natural Science Award (First Class) of Chinese Association of Automation.

Zonghai Chen (Senior Member, IEEE) was born in Anhui, China, in December 1963. He received the B.S. and M.E. degrees from the University of Science and Technology of China (USTC), Hefei, China, in 1988 and 1991, respectively.

He has been a Professor with the Department of Automation, USTC, since 1998. His main research interests include modeling and control of complex systems, intelligent robotic and information processing, energy management technologies for electric vehicles and smart microgrids.

Prof. Chen is a recipient of special allowances from the State Council of China. He is a member of the Robotics Technical Committee and Modelling, Identification and Signal Processing Technical Committee of the International Federation of Automation Control (IFAC).